Starch composites reinforced by bamboo cellulosic crystals

ARTICLE *in* BIORESOURCE TECHNOLOGY · DECEMBER 2009

Impact Factor: 4.49 · DOI: 10.1016/j.biortech.2009.11.058 · Source: PubMed

5 AUTHORS, INCLUDING:

Dagang Liu
Nanjing University of Information Science …
30 PUBLICATIONS **694** CITATIONS
SEE PROFILE

Tuhua Zhong
West Virginia University
13 PUBLICATIONS **123** CITATIONS
SEE PROFILE

Peter R. Chang
Agriculture and Agri-Food Canada
143 PUBLICATIONS **3,367** CITATIONS
SEE PROFILE

Bioresource Technology 101 (2010) 2529–2536

Contents lists available at ScienceDirect

Bioresource Technology

journal homepage: www.elsevier.com/locate/biortech

Starch composites reinforced by bamboo cellulosic crystals

Dagang Liu [a,c], Tuhua Zhong [a], Peter R. Chang [b,*], Kaifu Li [a], Qinglin Wu [c,*]

[a] College of Forestry, South China Agricultural University, Guangzhou 510642, People's Republic of China
[b] Agriculture and Agri-Food Canada, Biobased Platforms, Saskatoon, SK, Canada S7N 0X2
[c] School of Renewable Natural Resources, Louisiana State University Agricultural Center, Baton Rouge, LA 70803, USA

ARTICLE INFO

Article history:
Received 9 March 2009
Accepted 11 October 2009
Available online 16 December 2009

Keywords:
Bamboo cellulose crystals
Starch
Biocomposites

ABSTRACT

Using a method of combined HNO_3–$KClO_3$ treatment and sulfuric acid hydrolysis, bamboo cellulose crystals (BCCs) were prepared and used to reinforce glycerol plasticized starch. The structure and morphology of BCCs were investigated using X-ray diffraction, electron microscopy, and solid-state ^{13}C NMR. Results showed that BCCs were of typical cellulose I structure, and the morphology was dependent on its concentration in the suspension. BCC of 50–100 nm were assembled into leaf nervations at low concentration (i.e. 0.1 wt.% of solids), but congregated into a micro-sized "flower" geometry at high concentration (i.e. 10.0 wt.% of solids). Tensile strength and Young's modulus of the starch/BCC composite films (SBC) were enhanced by the incorporation of the crystals due to reinforcement of BCCs and reduction of water uptake. BCCs at the optimal 8% loading level exhibited a higher reinforcing efficiency for plasticized starch plastic than any other loading level.

1. Introduction

There is a growing interest in developing bio-based products and innovative processing technologies which offer sustainability and mitigation of the dependence on fossil fuel. Among biopolymers, starch is one of the most promising renewable bioresources due to its versatility, competitiveness in price, and applicability to various industries (Yang et al., 2007; Lenz, 1993; Pandey et al., 2005; John and Thomas, 2008). Through destructurization by the introduction of mechanical and heat energy or by incorporation of a plasticizing agent (e.g., water, amide, and/or polyols), starch can be processed into thermoplastic materials. Currently, biodegradable plastics are primarily used in food packaging films, shopping bags, and flushable sanitary product backing material (French and Murphy, 1976; Rhim, 2007; Kelfkens and Hamer, 1991). The use of starch-based materials is greatly hindered by its intractable nature, brittleness, water-sensitivity, and poor mechanical strength (Muller-Mangold, 1975; Liu and Zhang, 2006; Kumar et al., 2008; Liu et al., 2009). It has been found that using reinforcing materials in a starch matrix is an effective method to obtain high-performance starch-based biocomposites (Cao et al., 2008.). Various types of cellulose fillers such as jute fibers, eucalyptus pulp fibers, flax fiber, tunicin, and ramie fibers, have been prepared and used as reinforcing agents in biocomposites (John et al., 2007; Chakraborty et al., 2007).

Natural cellulosic nanocrystals have been gaining considerable interest because of their unique and attractive features (i.e. cost effectiveness, high aspect ratio, and light weight). Nevertheless, great differences exist in physical properties of various cellulose nanocrystals. These differences are mainly due to the different structures, sizes, and morphologies in the crystalline structures. During fiber extraction, chemical treatment removes surface wax, non-cellulosic substances, and degraded cellulosic compound(s), depending on the type and intensity of treatment. It was reported that normal cellulosic fibers from cornstalks, rice, and wheat straw are composed of single cells that are about 0.5–3.0 mm in length, whereas flax fiber is as long as 77 mm (Reddy and Yang, 2006, 2007). Cellulosic nanocrystals have a size of 2–50 nm in one-dimension (Dufresne, 2008; Kennedy et al., 2007). However, it is difficult to obtain uniformly dispersed cellulose nanocrystals from natural plant fibers, because the nano-phase has a strong tendency to form larger structures via aggregation and agglomeration. The structure, morphology, and crystallinity of the final crystals are greatly varied depending on crystal resources, pretreatments, temperatures, solvents, suspension or dry state, and other conditions.

Bamboo is a renewable natural bioresource abundant in many parts of the world. It has several advantages including small environment load, rapid growth, renewability, relatively high strength, and good flexibility. Bamboo fiber may play an important role in forming future organic structures and composites, and is recognized as an attractive candidate as a strengthening natural fiber; however, there is a lack of research in manufacture and use of cellulose crystals from bamboo. Understanding of the structure and morphology of bamboo cellulosic crystals could lead to more and

* Corresponding authors.
E-mail addresses: peter.chang@agr.gc.ca (P.R. Chang), wuqing@lsu.edu (Q. Wu).

0960-8524/$ - see front matter Crown Copyright © 2009 Published by Elsevier Ltd. All rights reserved.
doi:10.1016/j.biortech.2009.11.058

efficient utilization of this bioresource. In this study, a combined HNO_3–$KClO_3$ treatment and sulfuric acid hydrolysis method was used to extract nanocrystals from bamboo fibers. The objective of the study was to investigate the morphology and structure of the crystals, to combine the crystals with a hydrophilic starch matrix, and to analyze the properties of the composite.

2. Methods

2.1. Materials

Bamboo material used was Tonkin cane bamboo (*Pseudosasa amabilis,* also known as cha gan zhu in China) was obtained from Guangdong Province, China. Pea starch (PS; 84% starch, 6% protein, 2% fat, 2% ash, 7% moisture content), under the trade name of "Starlite" which is generated from pin-milling and air-classification of Canadian yellow pea, was procured from Parrheim Foods (Saskatoon, SK, Canada). Glycerol, nitric acid, sulfuric acid, and potassium chlorate were analytical grade reagents, which were purchased from Shenbo Reagent Company of Shanghai, China.

2.2. Preparation of bamboo fiber and cellulosic crystals

The HNO_3–$KClO_3$ method was used to extract fiber from the bamboo samples. Dry raw bamboo strands of 2 cm width and random length were immersed in 30% nitric acid aqueous solution. $KClO_3$ was added to the solution at a 10 wt.% ratio based on the weight of nitric acid. The weight ratio of bamboo strands was about 10 wt.%. After extracting for 24 h at 50 °C, the obtained bamboo fiber suspension was cooled and placed in regenerated cellulose dialysis membranes (MWCO of 14,000) and dialyzed against distilled water for 24 h to remove low molecular weight compounds. The slurry was then freeze–dried to obtain dry bamboo fiber, noted as BF. The yield of dry BF in relation to dry raw bamboo strands was about 45%. To produce nano-sized bamboo cellulosic crystals (BCCs), further acid hydrolysis was implemented. Briefly, the resulting bamboo fiber (about 40 g) was mixed with sulfuric acid (392 g, 50%). The slurry was stirred vigorously for 48 h, and then washed by dialysis in distilled water for 72 h. A 10% suspension of bamboo cellulosic crystals and a 0.1% suspension after further dilution were prepared and stored for further testing and analysis.

2.3. Preparation of starch/BCC composites

Starch and glycerol were first mixed and dispersed in distilled water. The mixture contained 6 wt.% pea starch, 2.4 wt.% glycerol and 91.6 wt.% water. The starch suspension was then poured into a round bottom flask equipped with a stirrer and heated at 80 °C for 30 min until the mixture gelatinized. Subsequently, the BCC dispersion with 10% concentration was added and the mixture was stirred for 20 min at 80 °C. After mixing, the mixture was degassed under vacuum, cast in a polystyrene mold, and dried in an oven at 40 °C. A series of starch/BCC composite films (SBC) of 0.4 mm thickness was prepared with 0, 1, 2, 3, 5, 8, 10, and 20 wt.% BCC loading rates were based on the PS matrix (dry weight basis). These samples were coded as PS, SBC1, SBC2, SBC3, SBC5, SBC8, SBC10, and SBC20, respectively. The composite films were kept at 0% *RH* (P_2O_5) for 1 week.

2.4. Characterization

Scanning electron microscopy (SEM) was performed to investigate the morphology of the BF, BCC, and SBC biocomposite films with an S-570 SEM (Hitachi, Japan) instrument. A drop of the suspension samples with 0.1% and 10% BCC concentrations was spread out on the glass plates, and then freeze–dried. BF and SBC samples were frozen in liquid nitrogen and then impact-fractured. The selected samples were mounted on SEM stands, coated with gold on an ion sputter coater, and observed at 20 kV by SEM. Transmission electron microscopy (TEM) observations were carried out on a JEOL JEM 2010 FEF (UHR) electron microscope with an accelerating voltage of 200 kV. One drop of BCC suspension was spread on the copper grid coated with carbon support film, and then coated with carbon for TEM observation.

Solid-state ^{13}C NMR spectra of freeze–dried BCC were recorded on an Infinity Plus-400 spectrometer (Varian Inc., USA; magnetic field = 9.4 T; ^{13}C frequency = 100.12 MHz) with a cross polarization/magic angle spinning (CP/MAS) unit at ambient temperature. Wide-angle X-ray diffraction (WAXD) patterns of the samples were recorded on a WAXD instrument (D/XRD-1200, Rigaku Denki, Japan) with Cu Kα radiation (λ = 0.154 nm) at 40 kV and 30 mA. X-ray diffraction data were collected from 2θ = 6 to 60° at a scanning rate of 4°/min. To determine the % crystallinity, the total diffracted area and the area under the crystalline peaks were determined by integration after correcting the data for absorption, Lorentz polarization effects, incoherent scatter, and air scatter. The ratio of the crystalline area to that of the total diffracted area was taken as the percent of crystallinity.

The SBC film samples were conditioned in desiccators with P_2O_5 as desiccant (0% relative humidity) at 25 °C to give an initial weight (W_0). After weighing, they were conditioned at 25 °C in desiccators with NaCl saturated aqueous solutions to provide a relative humidity (*RH*) of 75%. The samples were removed at specific time intervals and weighed with an analytical balance (0.0001 g accuracy) to give the sample weight W_t. The water content or water uptake (*WU*) of the samples was calculated using the following equation (Liu et al., 2008):

$$WU(\%) = \frac{W_t - W_0}{W_0} \times 100 \quad (1)$$

Tensile strength (σ_b), elongation at break (ε_b), and Young's modulus (E) of SBC films with dimensions of 50 × 10 × 0.4 mm (length × width × thickness), conditioned at 75% *RH*, were measured using a universal testing machine (CMT6503, Shenzhen SANS Test Machine Co. Ltd., Shenzhen, China) with a loading rate of 5 mm/min according to ISO527-3: 1995 (E). An average value of five replicates of each sample group was taken. Dynamic mechanical thermal analysis (DMTA) was carried out on a dynamic mechanical thermal analyzer (DMTA V, Rheometric Scientific Co.) in tension mode using 10 × 10 × 0.4 mm samples. The temperature was controlled from −50 to 250 °C using a heating ramp of 5 °C/min at a fixed frequency of 1 Hz.

3. Results and discussion

3.1. Structure of BCC

CP/MAS ^{13}C NMR spectra of the freeze–dried BCCs are shown in Fig 1. The BCCs exhibited five main peaks at 105.6, 89.2 (83.9), 74.5 (72.9) ppm [assigned to the C1, C4, C5 (C3, C2)], as well as the C6 peak line at 64.6 ppm, which were all attributed to cellulose I (Atalla and Vanderhart, 1999). The results strongly indicate that the BCC cellulose did not transform into another cellulose crystalline structure after being treated with combined HNO_3–$KClO_3$ and H_2SO_4 hydrolysis. In the literature, it is commonly assumed that higher plants synthesize both triclinic cellulose Iα and monoclinic cellulose Iβ. Their distinction lies simply in the different arrangements within the crystal lattice and in the way one parallel chain is stacked on the others. From the NMR data of this work, the C1

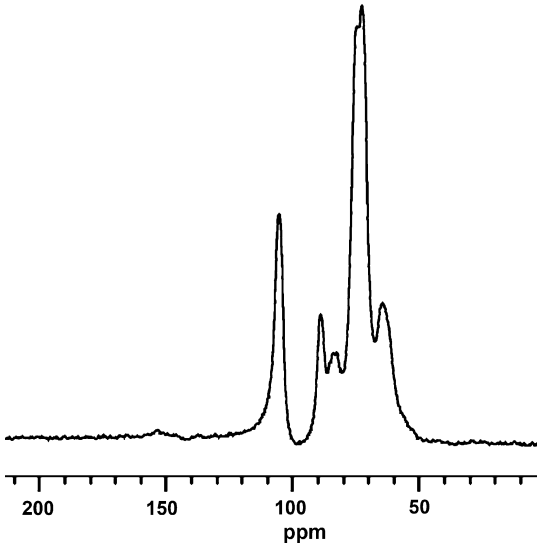

Fig. 1. CP/MAS ^{13}C NMR spectra of freeze–dried BCC.

resonance region at 105.6 ppm, C4 at 89.2 ppm, as well as C6 at 64.6 ppm are all attributed to cellulose Iβ. No obvious evidence of cellulose Iα (shoulder peak of C1 or C4) was found in the NMR which is consistent with the speculation/suggestion made by several researchers, i.e. higher plants contain no cellulose Iα at all, only a distorted form of cellulose Iβ located immediately below the surface of the crystalline units (Atalla and Vanderhart, 1984; Hesse-Ertelt et al., 2008).

X-ray diffraction is a powerful instrument for characterization of plant cellulose structure (Muller et al., 2002). The X-ray diffraction patterns for BCC are shown in Fig. 2. The diffraction peaks of the 2θ angles at about 22.7°, 16.1°, and 34.5° were assigned to the typical reflection planes of cellulose I, 002, 101, and 040, respectively. It was reported that alkaline treatment caused a decreasing intensity of the 002 plane and an increasing intensity of the 101 and 021 planes, representing the introduction of cellulose II. Interestingly, this phenomenon did not occur in the hydrolysis system used in this study. The intensity of 002 and 101 planes are very low probably because of the size effect of the BCC. In fact, crystalline units are about 2–3 nm (4–6 molecular chains) in width accompanied by many amorphous units in the plant cellulose crystals. They were therefore, too narrow to give low resolution diffraction data from micro-sized natural cellulose crystals after the acid or base hydrolysis processes. Only approximate unit cell dimensions can be obtained without any altered structure. The length (τ_{hkl}) of the crystal domains could be semi-quantitatively estimated using the Scherrer equation (Fink et al., 1995). The crystallite size of 002 and 101 planes were calculated to be 2.4 nm and 9.7 nm, respectively. The degree of crystallinity of BCC, calculated by the difference in the partial areas corresponding to the amorphous and crystalline portions of the trace obtained from WAXD, is 46.08%. The crystallite size and degree were all lower than those of reported natural fibers (Reddy and Yang, 2005).

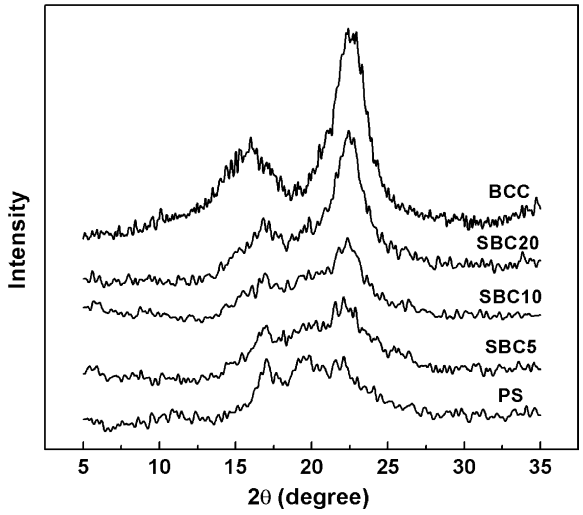

Fig. 2. Wide angle X-ray diffraction patterns for BCC and SBC.

3.2. Morphology of BF and BCC

SEM of BF and BCC freeze–dried from suspensions containing 10 wt.% and 0.1 wt.% solids are shown in Fig. 3. In this study, BF showed dimensions similar to those of other biomass (Chakraborty et al., 2007; Reddy and Yang, 2006, 2007). The lengths of single fiber were in the range of 0.01–1 mm, which is shorter than those of multicellular plant fibers such as flax, and the width was about 10–50 μm, as shown in Fig. 3a. After removing lignin and compounds of smaller molecular weight, the bamboo fiber had a rather smooth surface. After treatment with sulfuric acid the BF was degraded into crystals, as shown in Fig. 3b and c. BCC freeze–dried from suspension containing 0.1 wt.% solids seemed to be a leaf nervation composed of many sphere shaped nano-crystallites. The diameter of these smaller spherical crystallites was about 50–100 nm (inner of Fig. 3b). They were close to each other, but had a uniform distribution. On the other hand, many regimental flower arrays (with diameter of approximately 5 μm) were observed in BCC freeze–dried from suspension of 10 wt.% solids (Fig. 3c). The geometry of the crystals seemed to be defined by the concentration of crystals in suspension. Furthermore, the stability of the cellulose suspensions depended on the dimensions of the dispersed particles, their size polydispersity, and surface charge (Gousse et al., 2002; Samir et al., 2005). For sulfuric acid treated samples, a negatively charged surface seems to dominate the inter-crystal interactions. This type of cellulose nanocrystal was apt to conglomerate and stack into special micro-sized particles due to the surface electrostatic (Araki et al., 1999; Heux et al., 2000). TEM analysis of the suspension after acid hydrolysis revealed that BCCs had different geometries, dependent on its concentration in the suspension (Fig. 4). The morphology of freeze–dried crystals (50–100 nm) at low concentration, i.e. at 0.1 wt.% solids of BCC, appeared like a tree trunk with many branches (Fig. 4a). These particles could not withstand high voltage from the electron beam therefore high resolution TEM images could not be obtained from the carbohydrate polymer. However, crystals at high concentration, i.e. at 10.0 wt.% solids of BCC, exhibited a tendency to agglomerate, which can be observed by TEM in Fig. 4b. The X-ray diffraction pattern of the cellulose crystals in the selected area (inset Fig. 4b) produced two bright patterns attributed to 002 and 101 planes that are characteristic of oriented crystals, which correspond to the WAXD results (Yoshiharu et al., 1997).

3.3. Morphology of the SBC composites

Fig. 5 shows the SEM micrographs of neat glycerol plasticized pea starch and the BCC reinforced pea starch films. The fractured surface of neat starch films was rather smooth. After exposure to the electron probe for about 1 min, a few cracks appeared on the surface (Fig. 5a). When the starch matrix was filled with 1% BCC, small leaves were pulled out of the matrix surface, as shown in Fig. 5b. The inset photo in Fig. 5b shows a detailed leaf with a length of about 20 μm and a thickness of about 50 nm which ap-

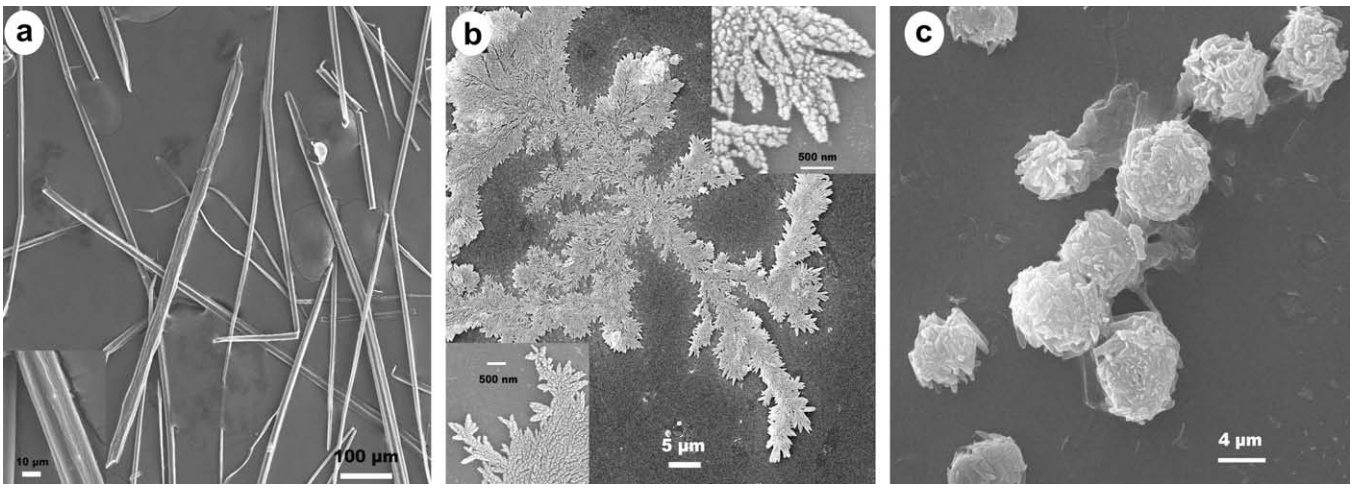

Fig. 3. SEM micrograph of freeze–dried bamboo fiber (a), BCC freeze–dried from suspensions with 0.1% (b) and 10% concentrations (c).

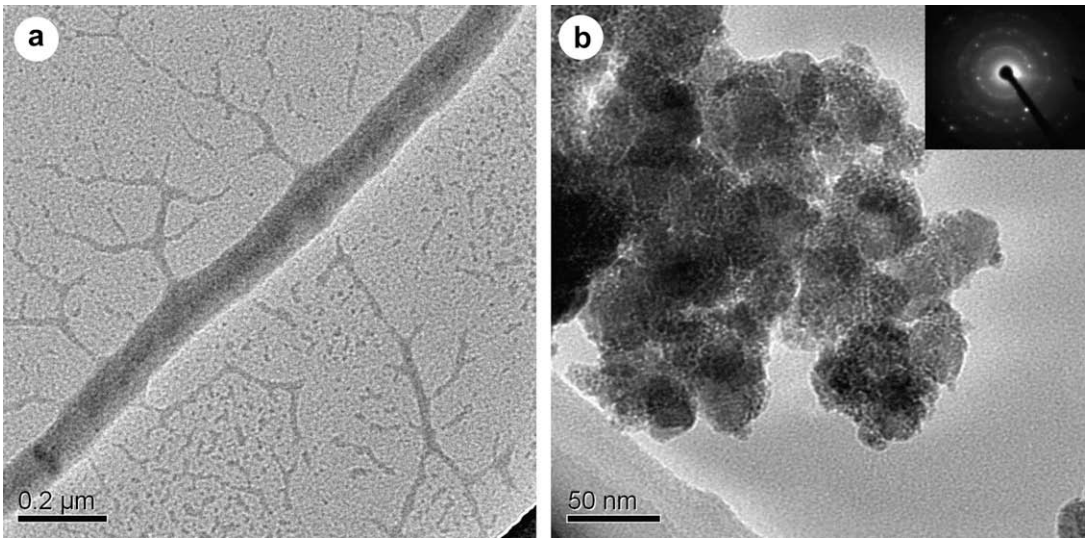

Fig. 4. TEM micrograph of freeze–dried BCC. (a) Freeze–dried from suspension with 0.1% concentration; (b) freeze–dried from suspension with 10% concentration. Inset of (b) is X-ray diffraction pattern of BCCs obtained using an area detector. The bright diffraction circles in the picture are due to orientation plane (0 0 2) and (1 0 1) of bamboo cellulose crystals.

peared from the crystallites. The leaves kept increasing on the rugged fracture surface, as indicated in Fig. 5c and d, due to good surface bonding between starch and low-level cellulose crystals. In sample SBC8, the leaf-like BCCs occurred infrequently, whereas the square particles increased (Fig. 5e). For Sample SBC10, the interface was smooth with white dots, which were distributed throughout the plasticized starch matrix (Fig. 5f). The size of the dot shaped particles matched that of the flowers as shown in Fig. 4b. When the BCCs loading level increased from 10% to 20%, the composites exhibited an increased concentration of congregated BCCs on the fractured surface (Fig. 5g and h).

SEM micrographs of BCCs and SBC show that the morphology of particles in composites with low BCC content is different from those with high BCC content. It is thought that as the concentration of crystals in the starch matrix increased, the available glycerol per existing crystal decreased. Polar glycerol played a role as solvent for the BCC in the composites during the casting process; therefore, at low concentration the suspended crystals kept their one-dimensional nano-size morphology and at high concentration levels, the crystals congregated into micro-particles. This was consistent with the morphology of the freeze–dried crystals as observed by SEM. Thus, at high concentrations it is difficult to prevent the self-congregation of BCCs from nano-size to micro-size during compounding with glycerol plasticized starch in the casting method.

3.4. Crystal structure of the composites

The X-ray diffraction patterns were also used to reveal the presence and characteristics of crystalline structures of SBC, as shown in Fig. 2. For the PS film, the 2θ angles at about 5.7°, 17.8°, 20.1°, and 22.6° were assigned to reflection planes of a typical C type crystallinity pattern, which is intermediate between the A type (cereal) and the B type (tuber) starch crystalline. It has been reported that all granules from pea starch contain both A and B polymorphs and that the B polymorphs are arranged centrally with the A polymorph located peripherally within the granules. The granules were oval shaped and were variable in size (2–40 μm) (Ratnayake et al., 2002), which was not observed in the plasticized starch film from Fig. 5a. The degree of crystallinity in pea starch was as low as 20.5%, which may be due to a low degree of crystalline order. When filled with cellulose crystals, the reflection plane of starch became weak accompanied by the increasing intensity of

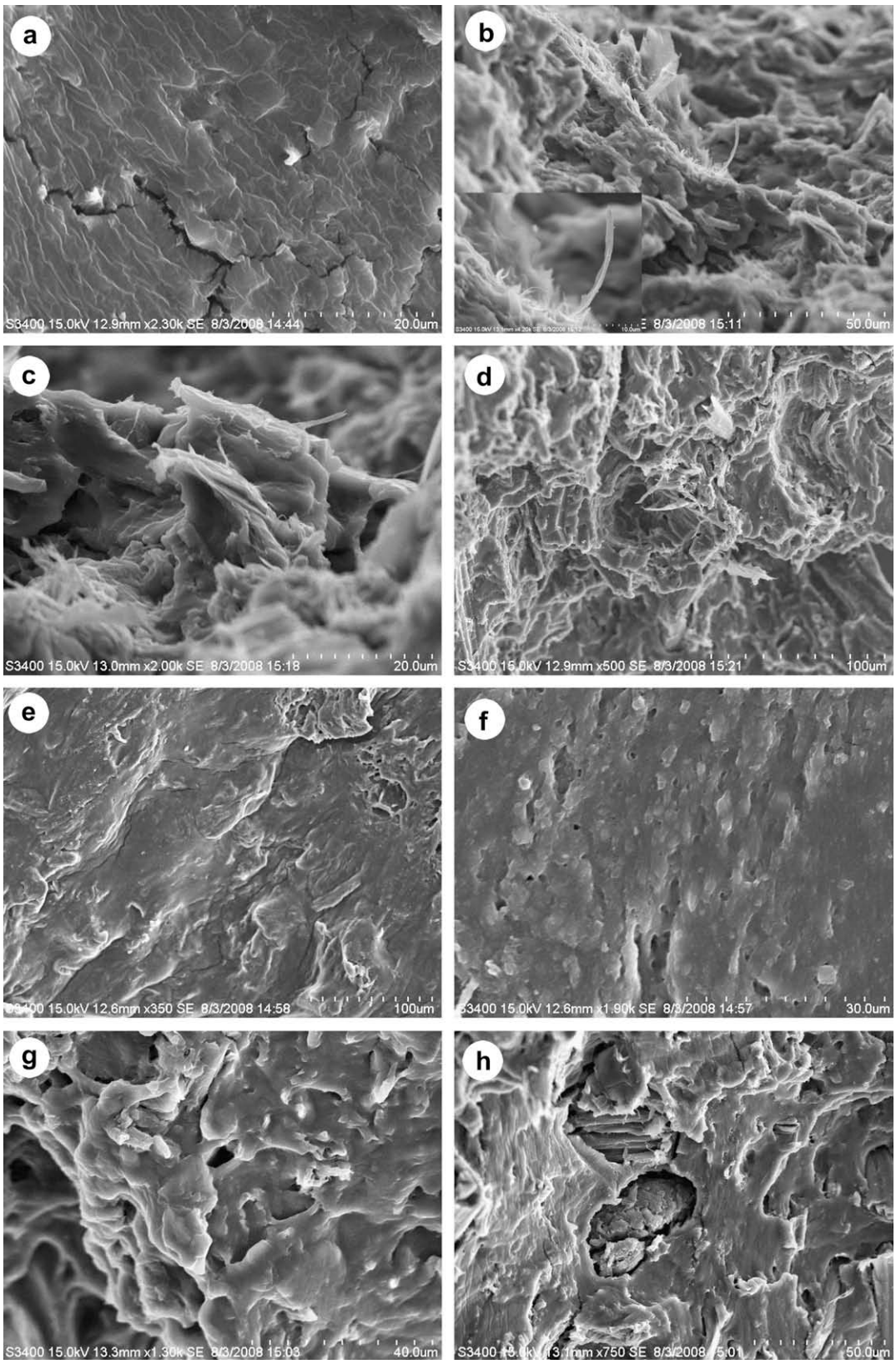

Fig. 5. SEM micrographs of plasticized pea starch and SBC films (a, PS; b, SBC1; c, SBC3; d, SBC5; e, SBC8; f, SBC10; g, SBC15; h, SBC20).

the cellulose I reflection plane from SBC5 and SBC10, to SBC20. Although BCCs maintained their original crystal style in the composites, they played an important role in elevating the degree of crystallinity of the composites. For example, the degree of crystallinity gradually increased from 24.8 in SBC5 and 28.5 in SBC10, to 36.4 in SBC20. For SBC20, the cellulose crystal was the dominant

crystal structure in the composites. Thus, it was deduced that the observed micro-particles on the fractured surface of SBC were not starch granules, but were attributed to the BCC crystals.

3.5. Mechanical properties of the SBC composites

Humidity is one of the most important factors affecting the mechanical properties of thermoplastic starch. For example, the mechanical strength of starch composites can reach 20 MPa in 0% *RH*; however, at high moisture conditions, the tensile strength may be below 1 MPa due to water plasticization (Lu et al., 2006; Glenn et al., 2007). Water uptake of the composites, from dry to the equilibrium condition at 75% *RH* is shown in Fig. 6. With the addition of BCCs, the water uptake of the SBC decreased. When the BCC content was greater than 8%, water uptake decreased very slowly. Water uptake of SBC20 was slightly higher than that of SBC15, which was probably due to the increasing interspace between BCC and starch, as evidenced by the SEM micrograph. Due to macro-phase separation caused by severe congregation of BCCs, more water could easily penetrate/diffuse into interspace. Mechanical properties of SBC conditioned at 75% *RH* (i.e. Young's modulus, tensile strength, and elongation at break) are shown in Fig. 7. When the BCC content increased from 0% to 8%, tensile strength and Young's modulus both increased sharply from 2.5 to 12.8 MPa, and from 20.4 to 210.3 MPa, respectively. The elongation at break increased when BCC content decreased. With increasing BCC content, both tensile strength and Young's modulus increased. When the size of particles was reduced enormously, many interesting phenomenon occurred as a result of the larger surface area and higher surface energy. Cellulose nanocrystals are reported to have a high modulus, up to 134 GPa, and strong tensile strength of more than 4 GPa (Sakurada et al., 1962). An 8% BCC content was quite sufficient to get a profound reinforcing effect comparable to starch composites reinforced with 30–50% cellulose fibers (Eichhorn et al., 2001; Bogoeva-Gaceva et al., 2007). When the BCC content was greater than 10%, interface adhesion was not sufficient to withstand the imposed high stretching forces, resulting in a decrease in tensile strength. Of course, decreased water uptake also accounted for the increases in modulus and strength of water-sensitive starch-based biocomposite.

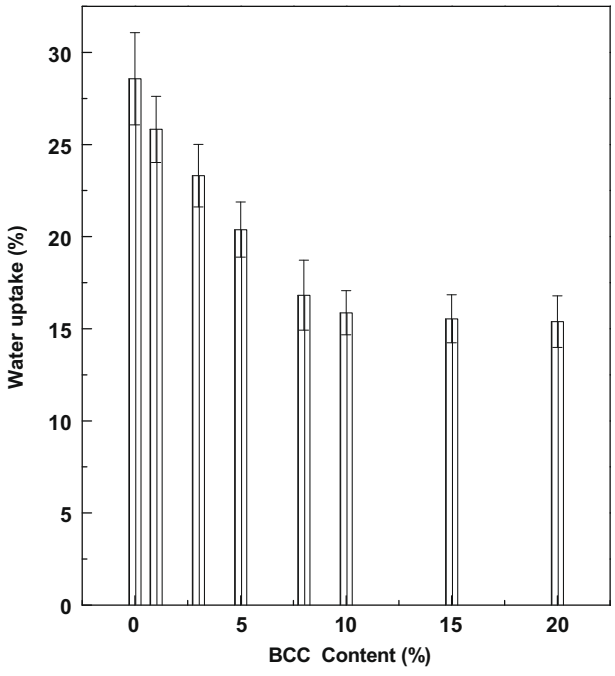

Fig. 6. Water uptake of plasticized pea starch and SBC at 75% *RH*.

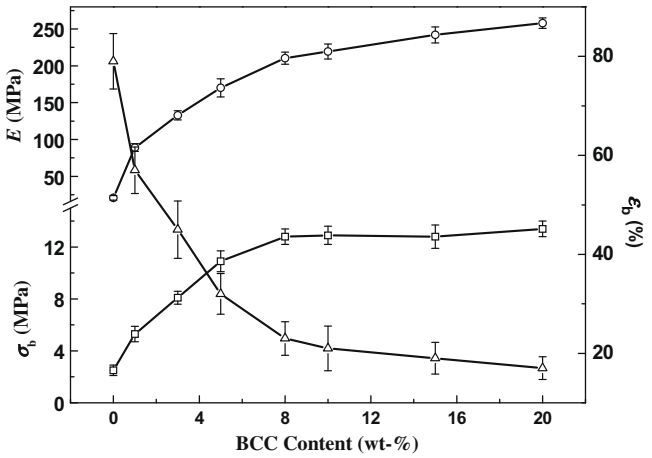

Fig. 7. Tensile strength (□), Young's modulus (○), and elongation at break (Δ) of plasticized pea starch and SBC at 75% *RH*.

As anticipated, DMTA reflected the reinforcing behavior of nano fillers. Temperature dependence on dynamic mechanical thermal behaviors for the starch composites is shown in Fig. 8 and the relaxation transition temperatures are listed in Table 1. In Fig. 8a

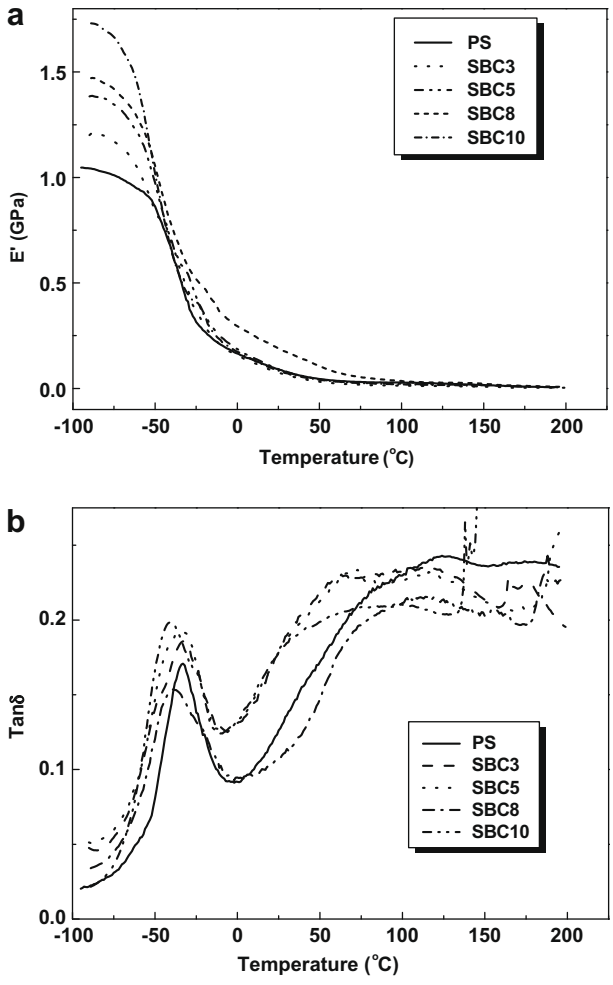

Fig. 8. Temperature dependence on a: storage module (*E*), and b: mechanical loss factor (tanδ) for the plasticized pea starch and SBC.

Table 1
Relaxation transition temperatures of plasticized PS and its SBC composites from DMTA.

Samples	$T\alpha 1$/°C	$T\alpha 2$/°C
PS	−33 ± 0.4	124 ± 1.1
SCN3	−33 ± 0.5	114 ± 0.8
SCN5	−34 ± 0.5	112 ± 1.4
SCN8	−39 ± 0.3	107 ± 0.9
SCN10	−41 ± 0.6	99 ± 1.2

the storage modulus, E', increased with increased BCC content due to the reinforcement of rigid crystals. At low temperature, the modulus of PS was about 1 GPa, and that of SBC was as high as 2 GPa. The modulus decreased quickly when the composite was at room temperature, which indicated a main relaxation transition. The modulus of the composite at 25 °C was only 10^2 MPa. After the relaxation transition was complete, the modulus tended to be stable. DMTA can also provide information about the relaxation mechanism correlated with the composition and microstructure of the composite (Zugenmaier, 2006). In Fig. 8b, two relaxation processes at lower (−40 to −20 °C) and higher (90–120 °C) temperature regions were attributed to the relaxation transitions of the glycerol rich domain and the starch rich domain, respectively (Mathew and Dufresne, 2002). An increase in tanδ with temperature indicated that the composites were becoming more viscous in nature with the rising temperature. When BCC content increased from 0 to 10 wt.%, the relaxation transition temperatures $T\alpha 1$ and $T\alpha 2$ had the same tendency to drift towards lower temperatures. It is thought that the strong interaction between starch molecules was weakened and starch chains moved easier due to the incorporation of cellulose crystals into the PS matrix, hence $T\alpha$ drifting to a lower temperature. The height of $T\alpha$ was considered to be related to the degree of crystallinity (Martin and Averous, 2001). Most of the composites exhibited a higher relaxation peak than starch, which is attributed to the incorporation of a significant quantity of cellulose crystals and their elevated degree of crystallinity.

4. Conclusions

Bamboo cellulose crystals were prepared using a combined HNO_3–$KClO_3$ treatment and sulfuric acid hydrolysis. The thus obtained nano-scaled crystals showed typical cellulose I structure, and the morphology was dependent on concentration in the suspension. At low concentration (i.e. at 0.1 wt.% solids of BCC), crystals of 50–100 nm assembled into leaf nervations; at high concentration (i.e. at 10.0 wt.% solids of BCC), crystals congregated into a micro-sized "flower" geometry. The different geometries resulting from aggregation intensity of BCCs were due to high surface electrostatic energy and large surface area. Tensile strength and Young's modulus of SBC8 were 12.8 and 210.3 MPa, respectively, which was much higher than their counterparts for glycerol plasticized-starch without bamboo crystals. Results from DMTA proved that the reinforcing effect of BCC on the starch composites was indeed due to size-effect and to the reduction of water uptake. The dispersion and polymorph of cellulose crystals were severely influenced by different treatments and the surrounding matrix, which ultimately affected the reinforcing effect on the plasticized starch-based biocomposites.

Acknowledgements

This work is financially supported by Natural Science Foundation of Guangdong Province (Doctor funding), China; the United States Department of Agriculture CSREES grant (68-3A75-6-508); and the CBIN program of Natural Resources Canada, Agricultural Bioproducts Innovation Program (ABIP) of Canada.

References

Araki, J., Wada, M., Kuga, S., Okana, T., 1999. Influence of surface charge on viscosity behavior of cellulose microcrystal suspension. J. Wood Sci. 45 (3), 258–261.
Atalla, R.H., Vanderhart, D.L., 1984. Native cellulose – a composite of two distinct crystalline forms. Science 223 (4633), 283–285.
Atalla, R.H., Vanderhart, D.L., 1999. The role of solid state ^{13}C NMR spectroscopy in studies of the nature of native celluloses. Solid State Nucl. Magn. Reson. 15 (1), 1–19.
Bogoeva-Gaceva, G., Avella, M., Malinconico, M., Buzarovska, A., Grozdanov, A., Gentile, G., Errico, M.E., 2007. Natural fiber eco-composites. Polym. Compos. 28 (1), 98–107.
Cao, X.D., Chen, Y., Chang, P.R., Stumborg, M., Huneault, M.A., 2008. Green composites reinforced with hemp nanocrystals in plasticized starch. J. Appl. Polym. Sci. 109 (6), 3804–3810.
Chakraborty, A., Sain, M., Kortschot, M., Cutler, S., 2007. Dispersion of wood microfibers in a matrix of thermoplastic starch and starch-polylactic acid blend. J. Biobased Mater. Bioenergy 1 (1), 71–77.
Dufresne, A., 2008. Polysaccharide nano crystal reinforced nanocomposites. Can. J. Chem. Rev. Can. Chim. 86 (6), 484–494.
Eichhorn, S.J., Baillie, C.A., Zafeiropoulos, N., Mwaikambo, L.Y., Ansell, M.P., Dufresne, A., Entwistle, K.M., Herrera-Franco, P.J., Escamilla, G.C., Groom, L., Hughes, M., Hill, C., Rials, T.G., Wild, P.M., 2001. Review: current international research into cellulosic fibres and composites. J. Mater. Sci. 36 (9), 2107–2131.
Fink, H.P., Hofmann, D., Philipp, B., 1995. Some aspects of lateral chain order in cellulosics from X-ray-scattering. Cellulose 2 (1), 51–70.
French, A., Murphy, V., 1976. Review of starch polymorphs. Cereal Food. World 21 (8), 429.
Glenn, G.M., Klamczynski, A., Holtman, K.M., Chiou, B.S., Orts, W.J., Wood, D., 2007. Cellulose fiber reinforced starch-based foam composites. J. Biobased Mater. Bioenergy 1 (3), 360–366.
Gousse, C., Chanzy, H., Excoffier, G., Soubeyrand, L., Fleury, E., 2002. Stable suspensions of partially silylated cellulose whiskers dispersed in organic solvents. Polymer 43 (9), 2645–2651.
Hesse-Ertelt, S., Witter, R., Ulrich, A.S., Kondo, T., Heinze, T., 2008. Spectral assignments and anisotropy data of cellulose I-alpha: ^{13}C-NMR chemical shift data of cellulose I-alpha determined by INADEQUATE and RAI techniques applied to uniformly 13C-labeled bacterial celluloses of different *Gluconacetobacter xylinus* strains. Magn. Reson. Chem. 46 (11), 1030–1036.
Heux, L., Chauve, G., Bonini, C., 2000. Nonflocculating and chiral-nematic self-ordering of cellulose microcrystals suspensions in nonpolar solvents. Langmuir 16 (21), 8210–8212.
John, M.J., Thomas, S., 2008. Biofibres and biocomposites. Carbohydr. Polym. 71 (3), 343–364.
John, M.J., Anandjiwala, R.D., Pothan, L.A., Thomas, S., 2007. Cellulosic fibre-reinforced green composites. Compos. Interface. 14 (7–9), 733–751.
Kelfkens, M., Hamer, R.J., 1991. Agronomic factors related to the quality of wheat for the starch industry. Part II: nitrogen-fertilisation and overall conclusions. Starch-Starke 43 (9), 344–347.
Kennedy, C.J., Cameron, G.J., Sturcova, A., Apperley, D.C., Altaner, C., Wess, T.J., Jarvis, M.C., 2007. Microfibril diameter in celery collenchyma cellulose: X-ray scattering and NMR evidence. Cellulose 14 (3), 235–246.
Kumar, R., Liu, D., Zhang, L., 2008. Advances in proteinous biomaterials. J. Biobased Mater. Bioenergy 2 (1), 1–24.
Lenz, R.W., 1993. Biodegradable polymers. Adv. Polym. Sci. 107, 1–40.
Liu, D., Zhang, L., 2006. Structure and properties of soy protein plastics plasticized with acetamide. Macromol. Mater. Eng. 291 (7), 820–828.
Liu, D., Tian, H., Zeng, J., Chang, P.R., 2008. Core-shell nanoblends from soy protein/polystyrene by emulsion polymerization. Macromol. Mater. Eng. 293 (8), 714–721.
Liu, D., Wu, Q., Chen, H., Chang, P.R., 2009. Transitional properties of starch colloids with particle size reduction from micro- to nanometer. J. Colloid Interf. Sci. 339 (1), 117–124.
Lu, Y., Weng, L., Cao, X., 2006. Morphological, thermal and mechanical properties of ramie crystallites – reinforced plasticized starch biocomposites. Carbohydr. Polym. 63 (2), 198–204.
Martin, O., Averous, L., 2001. Poly(lactic acid): plasticization and properties of biodegradable multiphase systems. Polymer 42 (14), 6209–6219.
Mathew, A.P., Dufresne, A., 2002. Morphological investigation of nanocomposites from sorbitol plasticized starch and tunicin whiskers. Biomacromolecules 3 (3), 609–617.
Muller, M., Hori, R., Itoh, T., Sugiyama, J., 2002. X-ray microbeam and electron diffraction experiments on developing xylem cell walls. Biomacromolecules 3 (1), 182–186.
Muller-Mangold, D., 1975. Review of 40 year experiences in starch industry. Starch-Starke 27 (6), 202–205.
Pandey, J.K., Kumar, A.P., Misra, M., Mohanty, A.K., Drzal, L.T., Singh, R.P., 2005. Recent advances in biodegradable nanocomposites. J. Nanosci. Nanotechnol. 5 (4), 497–526.
Ratnayake, W.S., Hoover, R., Warkentin, T., 2002. Pea starch: composition, structure and properties – a review. Starch-Starke 54 (6), 217–234.

Reddy, N., Yang, Y.Q., 2005. Structure and properties of high quality natural cellulose fibers from cornstalks. Polymer 46 (15), 5494–5500.
Reddy, N., Yang, Y.Q., 2006. Properties of high-quality long natural cellulose fibers from rice straw. J. Agric. Food Chem. 54 (21), 8077–8081.
Reddy, N., Yang, Y.Q., 2007. Natural cellulose fibers from switchgrass with tensile properties similar to cotton and linen. Biotechnol. Bioeng. 97 (5), 1021–1027.
Rhim, J.W., 2007. Potential use of biopolymer-based nanocomposite films in food packaging applications. Food Sci. Biotechnol. 16 (5), 691–709.
Sakurada, I., Nukushina, Y., Ito, T., 1962. Experimental determination of the elastic modulus of crystalline regions in oriented polymers. J. Polym. Sci. 57 (165), 651–660.
Samir, M.A.S.A., Alloin, F., Dufresne, A., 2005. Review of recent research into cellulosic whiskers, their properties and their application in nanocomposite field. Biomacromolecules 6 (2), 612–626.
Yang, K.K., Wang, X.L., Wang, Y.Z., 2007. Progress in nanocomposite of biodegradable polymer. J. Ind. Eng. Chem. 13 (4), 485–500.
Yoshiharu, N., Shigenori, K., Masahisa, W., Takeshi, O., 1997. Cellulose microcrystal film of high uniaxial orientation. Macromolecules 30 (20), 6395–6397.
Zugenmaier, P., 2006. Materials of cellulose derivatives and fiber-reinforced cellulose-polypropylene composites: characterization and application. Pure Appl. Chem. 78 (10), 1843–1855.